

# Signatures of Quantum-Corrected Black Holes in Gravitational Waves from Periodic Orbits

Fazlay Ahmed<sup>a,b,\*</sup>, Qiang Wu<sup>a,b,†</sup>, Sushant G. Ghosh<sup>c,d,‡</sup> and Tao Zhu<sup>a,b,§</sup>

<sup>a</sup>*Institute for Theoretical Physics & Cosmology, Zhejiang University of Technology, Hangzhou, 310023, China*

<sup>b</sup>*United Center for Gravitational Wave Physics (UCGWP),  
Zhejiang University of Technology, Hangzhou, 310023, China*

<sup>c</sup>*Centre for Theoretical Physics, Jamia Millia Islamia, New Delhi 110025, India*

<sup>d</sup>*Astrophysics and Cosmology Research Unit, School of Mathematics, Statistics and Computer Science,  
University of KwaZulu-Natal, Private Bag 54001, Durban 4000, South Africa*

(Dated: January 1, 2026)

We investigate gravitational wave emission from periodic timelike orbits of a test particle around a loop quantum gravity-inspired Schwarzschild black hole. The spacetime is characterised by a holonomy-correction parameter that modifies the radial metric component while preserving asymptotic flatness and the classical location of the horizon. The bound geodesics are systematically classified using the zoom-whirl representation labelled by three integers  $(z, w, v)$ . Gravitational waveforms are computed within a numerical framework that combines exact geodesic motion with the quadrupole approximation, which is suitable for extreme mass ratio inspirals. We demonstrate that the quantum corrections lead to distinct phase shifts, amplitude variations, and modifications to the harmonic structure of the waveforms, with increasingly complex features for orbits with larger zoom numbers. The corresponding frequency spectra and characteristic strain peak, which fall within the millihertz band, are within the sensitivity ranges of space-based detectors such as LISA, Taiji, and TianQin. For specific orbital configurations and values of the quantum-correction parameter, the characteristic strain exceeds the projected detector noise, indicating potential observability. Our results demonstrate that gravitational waves from periodic orbits provide a sensitive probe of quantum-corrected black hole spacetimes in the strong-field regime.

## I. INTRODUCTION

The detection of gravitational waves (GWs) by LIGO and Virgo in 2015 has revolutionised astronomy, steering in an exciting new era of cosmic exploration. This tremendous breakthrough not only deepens our understanding of the universe but also invites us to unlock its most profound mysteries [1–4]. Einstein’s general relativity (GR) first predicted it, which presents a distinctive observational window into the most energetic and violent cosmic events, such as binary black hole and binary neutron star mergers. Beyond these cataclysmic phenomena, the study of particle trajectories around black holes provides a robust theoretical framework for probing the intricate dynamics of strong gravitational fields. Among these trajectories, periodic orbits are particularly significant because they play a central role in addressing fundamental challenges in astrodynamics. The analysis of periodic orbits sheds light not only on the stability of celestial systems and the complex interactions between black holes and their surrounding matter, but also provides fundamental insights into generic orbital dynamics [5–8]. All generic orbits around black holes can be considered as minor deviations from periodic orbits [5]. The study of periodic orbits and their gravitational-wave

emissions is also of particular interest because of their potential observational applications in future space-based gravitational-wave detectors.

Black holes with stellar mass or neutron stars are often found in close orbits around supermassive black holes (SMBHs). Such binary systems are known as the extreme mass ratio inspiral (EMRI), being one of the most critical targets of future space-based gravitational detectors, such as Taiji [9], Tianqin [10, 11], LISA [12–16], etc. The examination of gravitational waveform features detected by these detectors allows for a precise reconstruction of the orbital dynamics of compact objects and the surrounding gravitational field of black holes, yielding key constraints on cosmic evolution and strong-field gravity [17, 18]. Given that the energy carried away by the orbital motion of the lower-mass object is an exceedingly small fraction of the total energy of the system, the time it takes for the smaller mass object to spiral around the supermassive black hole can span several years. During this process, the orbital dynamics of the smaller-mass object can be well approximated by periodic orbits.

A systematic classification of periodic orbits for massive particles provides valuable insight into the dynamical processes involved in black hole mergers [5]. The primary concept of this classification scheme is that a dynamic system can be understood by examining its periodic orbits. To be exact, three topological integers characterize periodic orbits around a black hole: zoom ( $z$ ), whirl ( $w$ ), and vertex ( $v$ ). Under this taxonomy, extensive research has been carried out on periodic orbits within various black hole spacetimes, to mention a few, including those of Schwarzschild and Kerr [6, 19–21], charged black hole

\* fazlayahmad12@gmail.com

† wuq@zjut.edu.cn

‡ sghosh2@jmi.ac.in

§ Corresponding author: zhut05@zjut.edu.cn

[7], naked singularities [8], Kerr-Sen black holes [22], and hairy black holes in Horndeski's theory [23]. For the studies of periodic orbits in other black holes, see refs. [24–48] and references therein. GWs emitted from periodic orbits exhibit distinct waveform features that encode specific orbital characteristics of the source. This connection has attracted considerable interest and motivated dedicated studies on gravitational-wave radiation from periodic orbits in a wide range of black hole spacetimes, see the references [29, 36, 49–72] and references therein.

It turns out GR successfully describes gravity on large scales, however it fails to explain the quantum nature of spacetime at small scales, which leaves essential questions unresolved and does not fully address singularity problems or quantum aspects of spacetime at the microscopic level [73]. To better understand these issues, researchers need to test and develop alternative theories. Spacetime singularities [74] remain a major challenge for classical general relativity. One way to address this is to modify black hole solutions to incorporate quantum effects. The Hamiltonian constraints approach [75] is a key framework for these modifications and has been important in the canonical quantization of general relativity. It is also important to determine whether quantum parameters can produce observable effects in current or future experiments, thereby enabling direct tests or limits on quantum effects in black hole spacetimes. With this in mind, researchers have already studied several observational and phenomenological effects of quantum-corrected black hole spacetimes [53, 76–84]. The direct detection of GWs and the EHT imaging of supermassive black holes (SMBHs) M87\* [85] and Sgr A\* [86] are major achievements in gravitational physics. These findings offer new insights into general relativity and many alternative theories of gravity. Building on these advances, we study the properties of periodic orbits and their generation of gravitational waveforms in a quantum-corrected black hole spacetime.

In this work, we investigate gravitational-wave (GW) emission arising from the periodic orbital motion of a test particle in the vicinity of a quantum-corrected Schwarzschild black hole. The primary objective is to investigate how quantum corrections to the Schwarzschild geometry may alter the structure of periodic orbits and imprint signatures on the resulting gravitational radiation. We use an effective quantum-corrected spacetime motivated by loop quantum gravity [73, 75] to examine deviations in orbital dynamics relative to general relativity and compute the corresponding GW waveforms within the numerical kludge approximation [14]. Our analysis indicates that quantum corrections in the background spacetime can lead to measurable changes in the phase, amplitude, and spectral content of the emitted GWs, potentially allowing future space-based detectors such as LISA, Taiji, and TianQin to probe quantum effects in the strong-gravity regime [9, 10, 15].

The paper is organised as follows: In Section II, we provide a brief review of the quantum-corrected

Schwarzschild black hole spacetime. Section III is devoted to the dynamics of massive test particles in this background metric, with particular emphasis on the properties of periodic bound orbits. In Section IV, we compute the gravitational-wave emission from these periodic trajectories and present the corresponding characteristic strain curves and Fourier spectra. Finally, Section V summarises our main results and discusses their physical implications.

## II. QUANTUM CORRECTED SCHWARZSCHILD BLACK HOLE

In this section, we give a brief review of static, spherically symmetric black hole solutions in quantum gravity. From this perspective, Loop Quantum Gravity (LQG) emerges as one of the most promising quantum gravity proposals, aiming to regularise gravity [73, 87, 88]. LQG is a non-perturbative theory for quantising the spacetime structure; however, it does not provide a complete quantum description of the removal of the singularity throughout spacetime. In this sense, one can investigate the effects of LQG in low-energy regimes through effective models, i.e., models that include corrections arising from quantum effects. Recently, in [89, 90], the authors obtained a solution of a regular, geodesically complete black hole, resulting from anomaly-free quantum corrections. Some aspects of this model have already been investigated, such as those linked to quasi-normal modes [91–95], gravitational lensing [80, 96–100], and horizon area [101].<sup>1</sup> In this work, we focus on gravitational radiation from periodic orbits around the quantum-corrected black hole. We begin with the line element [89, 90]

$$ds^2 = -A(r) dt^2 + \frac{r}{r - q_c} \frac{1}{A(r)} dr^2 + r^2 d\Omega^2, \quad (2.1)$$

with

$$A(r) = 1 - \frac{2M}{r}, \quad (2.2)$$

where  $M$  denotes the black hole mass and  $q_c$  is the holonomy-correction parameter, such that  $q_c < 2M$ . It is a static, spherically symmetric, and asymptotically flat spacetime. The spacetime (2.1) has a wormhole-like structure, with a minimal spacelike hypersurface separating the trapped regular black hole interior from the anti-trapped other region [112]. However, we consider light rays that do not cross the event horizon, characterised by  $r = r_h = 2M$ , i.e., we address regions with  $r > r_h$ . Though analytically, there is no clear difference

<sup>1</sup> The phenomenological implications of quantum effects arising from LQG with different quantized approaches have also been extensively explored in refs. [54, 83, 102–111] by several authors of this paper.

between the event horizon of a black hole defined in (2.1), and the standard Schwarzschild black hole, but there is a  $g^{rr}$  term that is significantly different in both spacetimes. This small difference arises from quantum corrections and has a significant impact on particle motion. This difference motivates us to analyse the black hole solution with some quantum corrections. However, in the absence of a well-established theory of quantum gravity, these quantum-corrected models are constructed within the framework of semiclassical gravity. The quantum-correction parameter defined in (2.1) is given by [112]:

$$q_c = 2M \frac{b^2}{1+b^2}, \quad (2.3)$$

where  $b$  is a dimensionless constant that is related to the fiducial length of the holonomies. It is worthwhile to mention that  $a$  defines a minimal spacelike hypersurface, whose area is  $4\pi r^2$ , separating the trapped black hole interior from the anti-trapped white hole region. The Komar, Arnowitt–Deser–Misner, and Misner–Sharp masses of the holonomy-corrected Schwarzschild black hole are given by [90]

$$\begin{aligned} M_K &= M \sqrt{1 - \frac{q_c}{r}}, \\ M_{ADM} &= M + \frac{q_c}{2}, \\ M_{MS} &= M + \frac{q_c}{2} - \frac{M q_c}{r}. \end{aligned} \quad (2.4)$$

In the limiting case  $q_c \rightarrow 0$  or  $b \rightarrow 0$ , the spacetime is reverted to the standard Schwarzschild black hole. It should be noted that the presence of the minimal spacelike hypersurface distinguishes the metric (2.1) from the standard Schwarzschild black hole; otherwise, both form the event horizon at  $r = 2M$ . Due to this, we can not differentiate the holonomy-corrected black hole from the Schwarzschild black hole, which motivates us to study the radial motion of the particle around the holonomy-corrected black hole, through which we can detect the difference through quantum corrections in the  $g_{rr}$  term.

### III. PERIODIC ORBITS

The periodic time-like orbits around a black hole in quantum-corrected geometry are covered in this section. To determine the complex structure of bound orbits in strong gravitational fields requires a brief review of periodic orbits [113]. Let us first consider the motion of a test particle in the background of a given black hole. The Lagrangian defines the dynamics of this particle and can be read

$$\mathcal{L} = \frac{1}{2} g_{\mu\nu} \frac{dx^\mu}{d\lambda} \frac{dx^\nu}{d\lambda}, \quad (3.1)$$

where  $\tau$  denotes the proper time, which serves as the affine parameter along the world line of a timelike particle. For a massless particle,  $\mathcal{L} = 0$ , while for a massive one  $\mathcal{L} < 0$ .

The corresponding generalized momentum  $p_\mu$  is given by

$$p_\mu = \frac{\partial \mathcal{L}}{\partial \dot{x}^\mu} = g_{\mu\nu} \dot{x}^\nu, \quad (3.2)$$

which leads to the following conserved quantities for a stationary and axisymmetric spacetime:

$$p_t = g_{tt} \dot{t} = -E, \quad (3.3)$$

$$p_\phi = g_{\phi\phi} \dot{\phi} = L, \quad (3.4)$$

$$p_r = g_{rr} \dot{r}, \quad (3.5)$$

$$p_\theta = g_{\theta\theta} \dot{\theta}, \quad (3.6)$$

where  $E$  and  $L$  represent, respectively, the conserved energy and angular momentum per unit mass of the particle. A dot denotes differentiation with respect to the affine parameter  $\lambda$ .

From these definitions, we obtain

$$\dot{t} = -\frac{E}{g_{tt}} = \frac{E}{A(r)}, \quad (3.7)$$

$$\dot{\phi} = \frac{L}{g_{\phi\phi}} = \frac{L}{r^2 \sin^2 \theta}. \quad (3.8)$$

For timelike geodesics, the normalisation condition

$$g_{\mu\nu} \dot{x}^\mu \dot{x}^\nu = -1 \quad (3.9)$$

must hold. Substituting Eqs. (3.7) and (3.8) into this relation yields

$$\begin{aligned} g_{rr} \dot{r}^2 + g_{\theta\theta} \dot{\theta}^2 &= -1 - g_{tt} \dot{t}^2 - g_{\phi\phi} \dot{\phi}^2 \\ &= -1 + \frac{E^2}{A(r)} - \frac{L^2}{r^2 \sin^2 \theta}, \end{aligned} \quad (3.10)$$

which defines the radial and polar motion of a test particle in the background of a quantum-corrected black hole. The systematic analysis of these orbits provides a natural framework for classifying zoom-whirl periodic trajectories and investigating their potential observational signatures in quantum-corrected black hole [6, 7, 113].

Here, we are interested in the motion of particles in equatorial circular orbits. For simplicity, we choose  $\theta = \pi/2$  and  $\dot{\theta} = 0$ . Then the above expression can be simplified into the form

$$\dot{r}^2 = (1 - q_c/r)(E^2 - V_{\text{eff}}(r)), \quad (3.11)$$

where  $V_{\text{eff}}(r)$  denotes the effective potential and is given by

$$V_{\text{eff}}(r) = \left(1 + \frac{L^2}{r^2}\right) A(r). \quad (3.12)$$

It is evident that  $V_{\text{eff}}(r) \rightarrow 1$  as  $r \rightarrow +\infty$ , as expected for an asymptotically flat spacetime. In this case, particles with energy  $E > 1$  can escape to infinity. The case  $E = 1$  is the critical point between bound and unbound

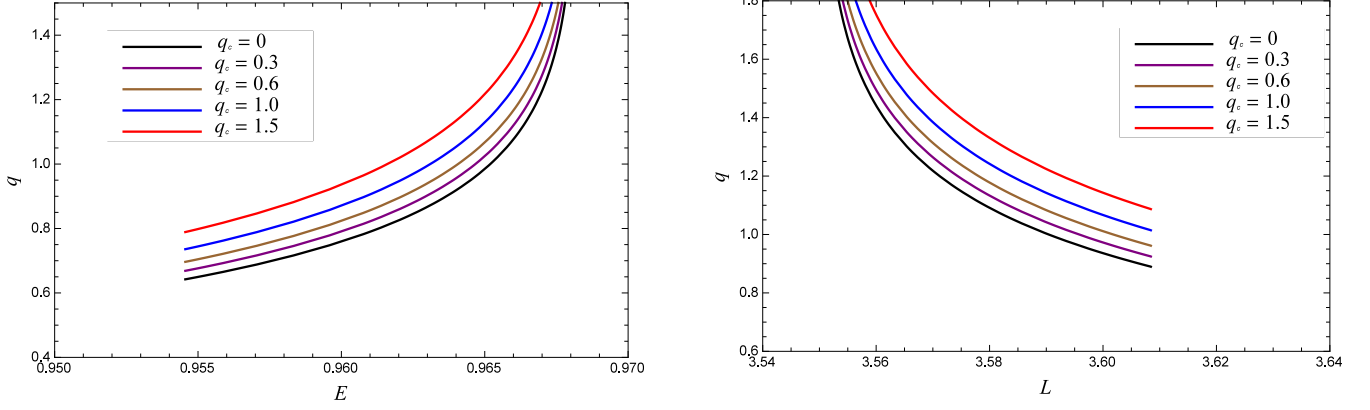


FIG. 1. The figure demonstrates the dependence of the rational number  $q$  on the energy (left panel) and orbital angular momentum (right panel) for different values of the parameter  $q_c$ . Here, we set  $L = 3.73$  and  $E = 0.95$  for the left and right panels, respectively.

orbits. Thus, the maximum energy that can bind a particle in orbits is  $E = 1$ . We can obtain the trajectory of a particle by solving Eqs. (3.7), (3.8), and (3.12) to get  $t$ ,  $\phi$ , and  $r$  as functions of  $\tau$ . However, since Eq. (3.11) involves taking a square root, the choice of sign corresponds to whether the particle is going inward or outward, and must be specified manually before any numerical integration. A convenient equation of motion, derived from the  $r$ -component of the geodesic equation, can be used for numerical analysis:

$$\ddot{r} = \frac{A'(r)(1 - q_c/r) + A(r)q_c/r^2}{2(1 - q_c/r)A(r)} \dot{r}^2 - \frac{A'(r)(1 - q_c/r)E^2}{2A(r)} + \frac{A(r)(1 - q_c/r)L^2}{r^3}. \quad (3.13)$$

This equation is utilized for numerical integration and helps in examining the stability of circular orbits, as well as how they evolve into periodic or zoom-whirl trajectories in strong gravitational fields [6, 7, 113, 114].

After completing the integration, a periodic orbit can be obtained for specific values of  $E$  and  $L$ , which is a bound trajectory that returns exactly to its initial position after a fixed period. Such orbits can take various shapes, depending on the energy and angular momentum of the particle. To study them systematically, it is convenient to use a classification scheme.

We utilized the approach introduced by Levin and Perez Giz [5], which classifies all periodic orbits around black holes using a representation of  $(z, w, v)$ , corresponding to the zoom, whirl, and vertex behavior of the trajectory. In this methodology, a periodic orbit returns to its initial position after a finite time, which implies that the ratio of the radial to azimuthal frequencies is rational. Because a rational one can approximate any irrational number, periodic orbits can effectively represent generic bound trajectories around black holes. The Levin and Perez-Giz [5] method has been successfully applied to various black holes, including Schwarzschild and

Kerr geometries [6–8], and is a valuable methodology for studying the corresponding GW forms from these orbits.

According to the representations of [5], the ratio  $q$  between the two frequencies  $\omega_r$  and  $\omega_\phi$  of oscillations in the  $r$ -motion and  $\phi$ -motion, respectively, in terms of three integers  $(z, w, v)$  as

$$q \equiv \frac{\omega_\phi}{\omega_r} - 1 = w + \frac{v}{z}. \quad (3.14)$$

The integers  $(z, w, v)$  each have different geometric interpretations. The zoom number  $z$  counts the larger circles in an orbit, and the whirl number  $w$  counts the small loops near the black hole. The vertex number  $v$  shows whether the particle moves through the orbit's vertices in a clockwise or anti-clockwise direction. To avoid degeneracy,  $z$  and  $v$  should be relatively prime [5]. The parameter  $q$  quantifies the deviation of the orbit from a simple ellipse and characterizes its shape. This approach also looks at the order in which the orbital paths or segments are traced. Together, these numbers describe the complex behavior of periodic orbits. The ratio  $\frac{\omega_\phi}{\omega_r}$  is equal to  $\Delta\phi/(2\pi)$ , where  $\Delta\phi = \oint d\phi$  is the total equatorial angle for one period in  $r$ , and this must be a multiple of  $2\pi$ . Using the geodesic equations for quantum-corrected black holes, we can calculate  $q$  as follows:

$$\begin{aligned} q &= \frac{1}{\pi} \int_{r_1}^{r_2} \frac{\dot{\phi}}{\dot{r}} dr - 1 \\ &= \frac{1}{\pi} \int_{r_2}^{r_1} \frac{L}{r^2 \sqrt{(1 - q_c/r)(E^2 - V_{\text{eff}}(r))}} dr - 1, \end{aligned} \quad (3.15)$$

where  $r_1$  and  $r_2$  are two turning points.

Fig. 1 illustrates the relationship between  $q$ ,  $E$ , and  $L$ . The results indicate that energy  $E$  increases monotonically with  $q_c$ , while angular momentum  $L$  decreases as  $q_c$  increases. It is evident that the Energy  $E$  and the

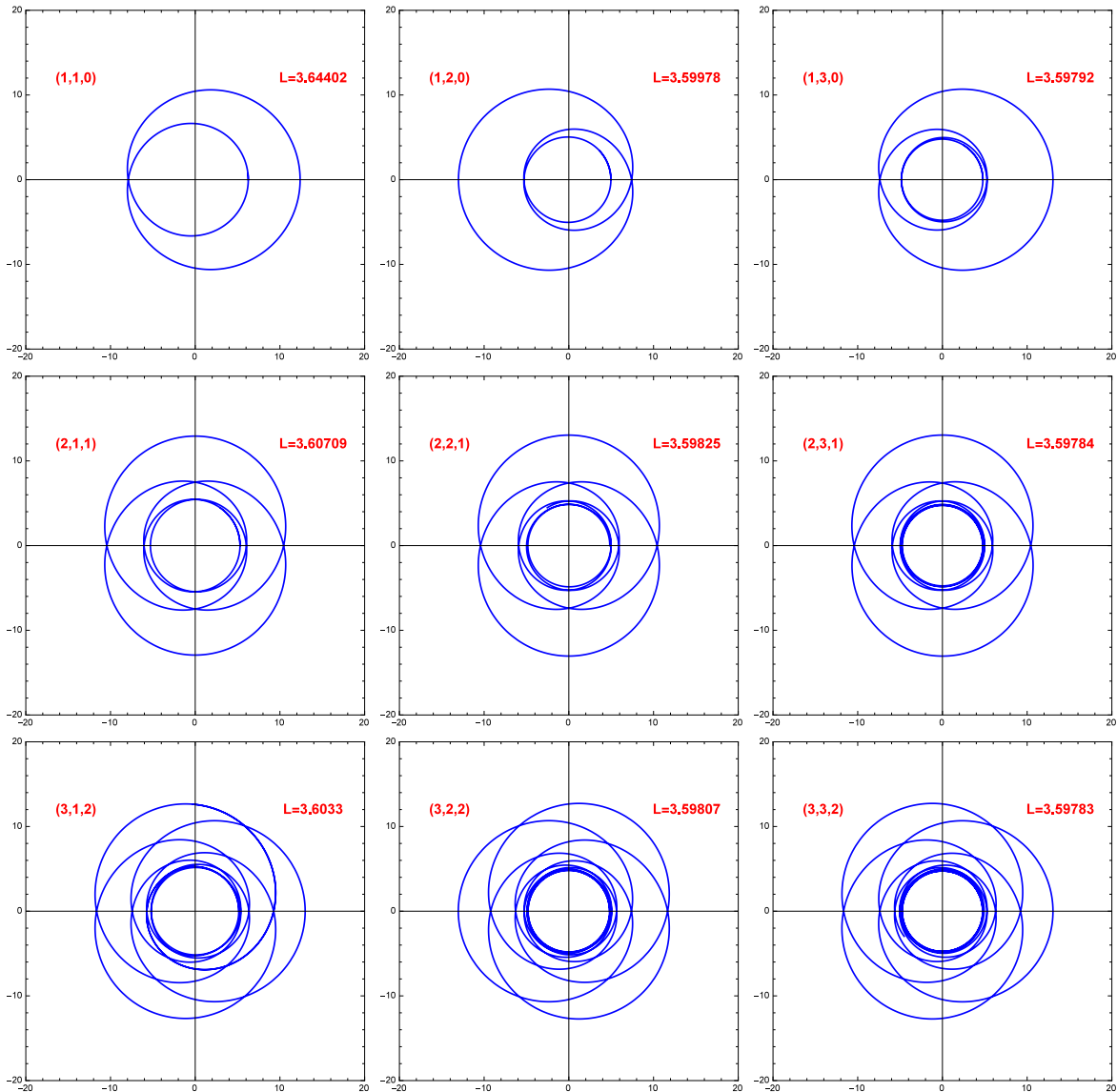


FIG. 2. Periodic orbits around a quantum-corrected black hole. The particle energy is fixed at  $E = 0.95$ . Each trajectory corresponds to a different set of zoom-whirl-vertex numbers  $(z, w, v)$ , illustrating the geometric complexity and structure of the bound periodic orbits.

angular momentum  $L$  are confined to a small region, and outside these, no other values are valid for our analysis. These numerical values of  $E$  and  $L$  play a crucial role in determining the periodic orbits. In Figs. 2 and 3, we illustrate the periodic orbits of quantum-corrected black holes for different combinations of integers  $(z, w, v)$ . The value of  $z$  determines the number of blades in the orbit's shape. The larger  $z$  values correspond to larger blade profiles and increasingly complex trajectories. In Fig. 2, we keep the energy fixed, while in Fig. 3, we fix the angular momentum. Note that we set  $M = 1$  for simplicity in the figures.

#### IV. GRAVITATIONAL RADIATION IN QUANTUM-CORRECTED GEOMETRY

Next, we analyze the gravitational radiation emitted by a test particle moving in periodic orbits around SMBHs, assuming that it is quantum-corrected. The EMRIs, consisting of a stellar-mass compact object orbiting an SMBH, are among the most promising sources for future space-based GW detectors such as LISA, Taiji, and TianQin [9, 11, 15]. The GWs generated by these systems encode detailed information about the strong-field dynamics and the underlying spacetime geometry of the central black hole. If successful, future observations could reveal quantum effects in black hole spacetimes, making this research highly relevant for upcoming



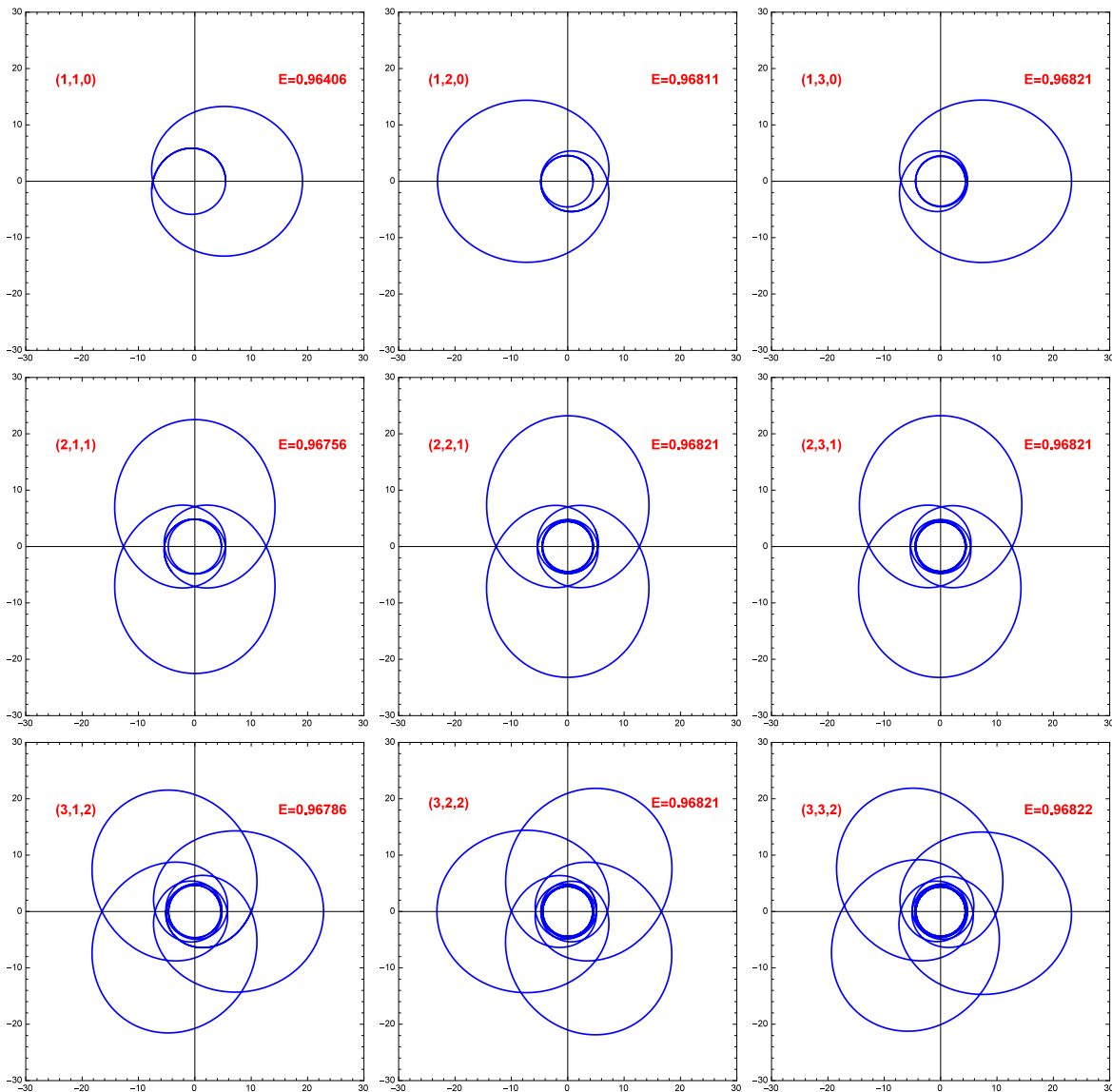


FIG. 3. Periodic orbits for various  $(z, w, v)$  combinations around a quantum-corrected black hole. Here, we fixed the angular momentum at  $L = 3.73$ .

experimental efforts.

Exploration of GWforms from EMRIs is typically carried out using the adiabatic approximation, which supposes that the inspiral timescale is much longer than the orbital period [115, 116]. The motion of the smaller object can be described as a series of geodesics with respect to the background metric, since its energy and angular momentum change slowly in this regime. For short-term orbital revolution [117], the radiation response, or back-reaction of the emitted GWs on the particle's motion, could be neglected at leading order.

We used a waveform model that provides a practical approach to computing the GWs emitted by periodic orbits in a black hole spacetime, following the framework developed in [118]—generally known as the numerical kludge scheme, which proceeds in two main steps. First,

the motion of the small compact object is obtained by numerically solving the geodesic equations in the background spacetime of the black hole. In the second step, the corresponding gravitational waveform is constructed using the standard quadrupole formula for gravitational radiation. This semi-relativistic approximation has been widely employed to model GW signals from EMRIs and provides a powerful tool for analyzing the dynamics of the orbit, the properties of the central black hole, and possible environmental effects [14, 116, 119]. For a metric perturbation  $h_{ij}$  representing the GW and a symmetric trace-free (STF) mass quadrupole moment  $I_{ij}$ , the quadrupole formula takes the form

$$h_{ij} = \frac{1}{A} \ddot{I}_{ij}, \quad (4.1)$$

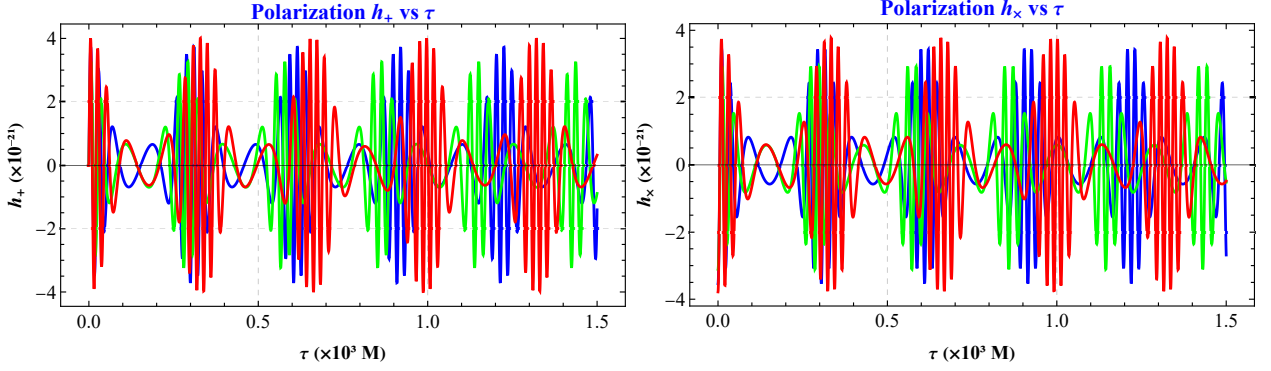


FIG. 4. GWforms (plus and cross polarizations) generated by a test particle of mass  $m = 10M_\odot$  in periodic orbits characterized by  $(z, w, v) = (1, 2, 0)$  (blue),  $(2, 1, 1)$  (green), and  $(3, 2, 2)$  (red) around a supermassive black hole of mass  $M = 10^6 M_\odot$ . The quantum-correction parameter is  $q_c = 0.6$  and  $E = 0.95$ . Distinct zoom-whirl phases in the orbital motion are reflected in the modulation of the waveform amplitude and frequency.

where  $A = c^4 D_L / (2G)$ ,  $G = c = 1$ , and  $D_L$  is the luminosity distance to the source. By numerically integrating the geodesic equations, one obtains the trajectory  $Z_i(t)$  of the small object in the curved spacetime of the supermassive black hole, which is then used to compute the GW signal. For a particle of mass  $m$  moving along a trajectory  $Z^i(t)$ , the quadrupole moment  $I_{ij}$  is defined as [120]

$$I^{ij} = m \int d^3x x^i x^j \delta^3(x^i - Z^i(t)). \quad (4.2)$$

The choice of coordinate system has a significant role in both the computation and interpretation of gravitational waveforms. While the geodesic equations are usually solved in the coordinates  $(r, \theta, \phi)$ , the resulting waveform is conveniently expressed in detector-based Cartesian coordinates  $(X, Y, Z)$ , which simplifies the analysis of the signal measured by a gravitational-wave detector. The coordinate transformation is given by [118]

$$x = r \sin \theta \cos \phi, \quad y = r \sin \theta \sin \phi, \quad z = r \cos \theta. \quad (4.3)$$

This transformation enables us to project the small-object trajectory onto a Cartesian grid, which is essential to evaluate the source multipole moments. The metric perturbations  $h_{ij}$ , representing the emitted GWs, are then computed from the second time derivative of the mass quadrupole moment  $I_{ij}$  as

$$h_{ij} = \frac{m}{A} (a_i x_j + a_j x_i + 2v_i v_j), \quad (4.4)$$

where  $v_i$  and  $a_i$  denote the velocity and acceleration components of the small object, respectively, and  $A = c^4 D_L / (2G)$  with  $G = c = 1$ . This formalism adheres to the conventional numerical kludge waveforms [14, 116, 118, 119], a practical, effective, and physically consistent approach to computing EMRI waveforms.

To analyze the gravitational-wave signal recorded by a detector, it is convenient to introduce a detector-adapted Cartesian coordinate system  $(X, Y, Z)$ , centred on the

black hole and oriented with respect to the source frame  $(x, y, z)$  by the inclination angle  $\iota$  and the longitude of pericentre  $\zeta$  [14, 116, 118]. This transformation facilitates the projection of the waveform onto the detector frame, enabling the computation of the observable GW polarizations. The unit vectors of the detector frame in the  $(x, y, z)$  coordinates are:

$$\hat{e}_X = (\cos \zeta, -\sin \zeta, 0), \quad (4.5)$$

$$\hat{e}_Y = (\sin \iota \sin \zeta, \cos \iota \cos \zeta, -\sin \iota), \quad (4.6)$$

$$\hat{e}_Z = (\sin \iota \sin \zeta, -\sin \iota \cos \zeta, \cos \iota), \quad (4.7)$$

The GW polarizations  $h_+$  and  $h_\times$  are then obtained by projecting  $h_{ij}$ , Eq. (4.4), onto the detector frame

$$h_+ = \frac{1}{2} (e_X^i e_X^j - e_Y^i e_Y^j) h_{ij}, \quad (4.8)$$

$$h_\times = \frac{1}{2} (e_X^i e_Y^j - e_Y^i e_X^j) h_{ij}, \quad (4.9)$$

These polarizations can be expressed in terms of components  $h_{\zeta\zeta}$ ,  $h_{\iota\iota}$ , and  $h_{\iota\zeta}$ , which are defined in the detector frame as combinations of the  $h_{ij}$  components as

$$h_+ = \frac{1}{2} (h_{\zeta\zeta} - h_{\iota\iota}), \quad (4.10)$$

$$h_\times = h_{\iota\zeta}, \quad (4.11)$$

where the components are [118]

$$h_{\zeta\zeta} = h_{xx} \cos^2 \zeta - h_{xy} \sin 2\zeta + h_{yy} \sin^2 \zeta, \quad (4.12)$$

$$h_{\iota\iota} = \cos^2 \iota [h_{xx} \sin^2 \zeta + h_{xy} \sin 2\zeta + h_{yy} \cos^2 \zeta] + h_{zz} \sin^2 \iota - \sin 2\iota [h_{xz} \sin \zeta + h_{yz} \cos \zeta], \quad (4.13)$$

$$h_{\iota\zeta} = \frac{1}{2} \cos \iota [h_{xx} \sin 2\zeta + 2h_{xy} \cos 2\zeta - h_{yy} \sin 2\zeta] + \sin \iota [h_{yz} \sin \zeta - h_{xz} \cos \zeta]. \quad (4.14)$$

To examine the influence of the quantum-correction parameter on gravitational waveforms generated by different periodic orbits in an EMRI system, we consider a compact object of mass  $m = 10 M_\odot$  orbiting a supermassive black hole (SMBH) of mass  $M = 10^6 M_\odot$ . For

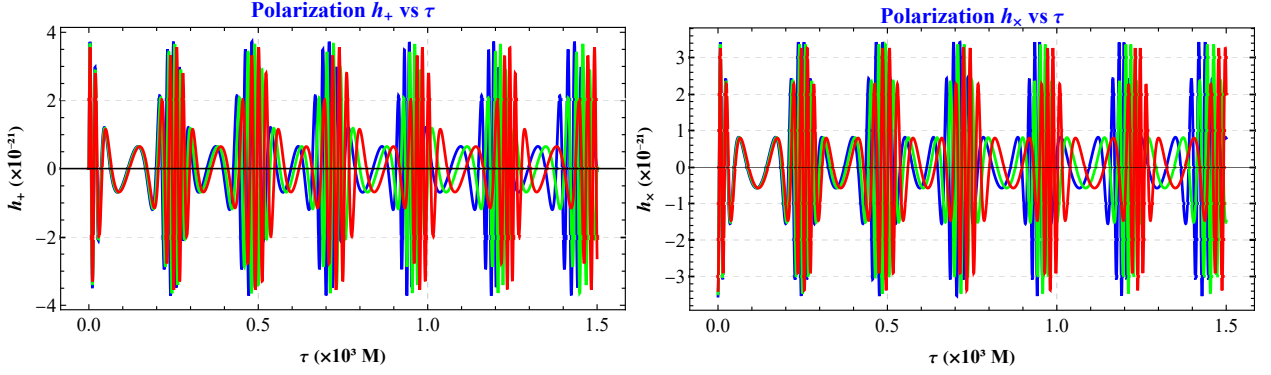


FIG. 5. Gravitational waveforms from a test object with  $m = 10M_\odot$  around periodic orbits with quantum-correction parameter  $q_c = 0.6$ : blue, 1.0: green, and 1.5: red, around a supermassive black hole with mass  $M = 10^6 M_\odot$ . The zoom-whirl value of the periodic orbit is  $(1, 2, 0)$ , and energy is fixed at  $E = 0.95$ . The left and right panels correspond to plus and cross polarizations, respectively.

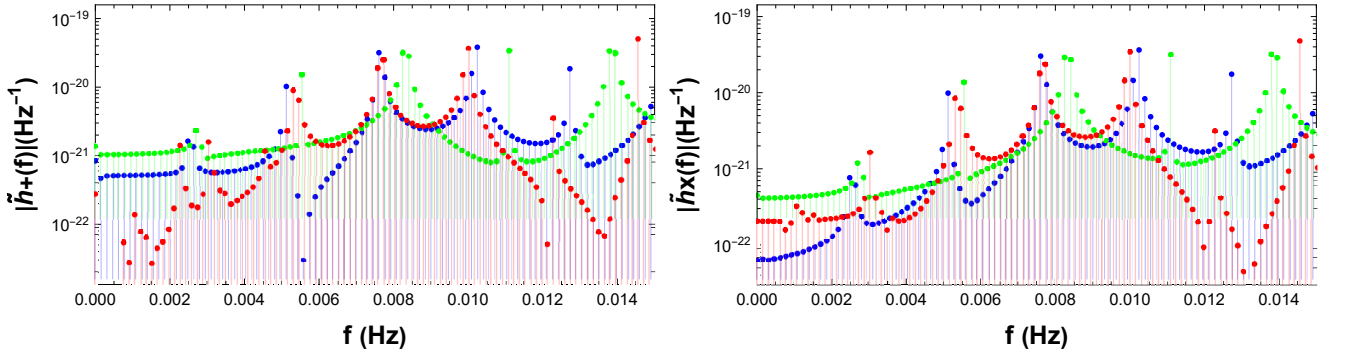


FIG. 6. Fourier spectra  $|\tilde{h}_{+, \times}(f)|$  corresponding to the time-domain waveforms shown in Fig. 4 for  $q_c = 0.6$ . The spectral peaks correspond to characteristic frequencies of the zoom-whirl orbits, showing distinct harmonic structures related to the orbital parameters  $(z, w, v)$ .

simplicity, the inclination angle  $\iota$  and the longitude of pericentre  $\zeta$  are fixed at  $\pi/4$ , and a luminosity distance of  $D_L = 200$  Mpc is adopted for the computation of the GW polarizations.

The resulting gravitational waveforms, represented by the two independent components  $h_+$  and  $h_\times$ , exhibit a characteristic alternating pattern. During the portions of the orbit where the trajectory extends outward in a highly eccentric fashion (the zoom phases), the waveform amplitude remains relatively low. These intervals are followed by short, intense bursts of radiation associated with the nearly circular segments of the trajectory (the whirl phases). The number of low-amplitude intervals corresponds to the number of zoom segments, while the number of intense bursts matches the number of whirls in the orbit. The numerical results obtained from Eqs. (4.10) and (4.4) are shown in Figs. 4 and 5, which clearly display the distinct “zoom” and “whirl” features of the GW signal from periodic orbits in EMRIs, reflecting the orbital dynamics of the small object over one complete cycle [5, 14, 116, 118].

In Fig. 4, the gravitational waveforms are shown with  $(z, w, v) = (1, 2, 0), (2, 1, 1)$  and  $(3, 2, 2)$ . This analysis

reveals a strong correlation between gravitational waveforms and the orbital motion of the small object. Each orbit displays clear “zoom” and “whirl” phases in the waveform that mirror the corresponding behaviors in the object’s trajectory. Additionally, orbits with higher zoom numbers  $z$  produce waveforms with more intricate substructures, reflecting the increased number of “leaves” in the complete periodic orbit.

The presence of the quantum-correction parameter  $q_c$  has a pronounced effect on the gravitational waveform generated by a massive particle moving in a periodic orbit. In Fig. 5, we have shown the impact of parameter  $q_c$  using its different values. Our study indicates that the gravitational waveforms exhibit substantial amplitude changes and a discernible phase shift as  $q_c$  increases, demonstrating the impact of spacetime quantum corrections on orbital dynamics and the resulting radiation.

The GWs emitted by a test particle in periodic motion around an SMBH in a quantum-corrected spacetime can be further analyzed through their frequency spectra  $|\tilde{h}_{+, \times}(f)|$  and characteristic strain  $h_c(f)$ , defined as

$$h_c(f) = 2f \left( |\tilde{h}_+(f)|^2 + |\tilde{h}_\times(f)|^2 \right)^{1/2}. \quad (4.15)$$



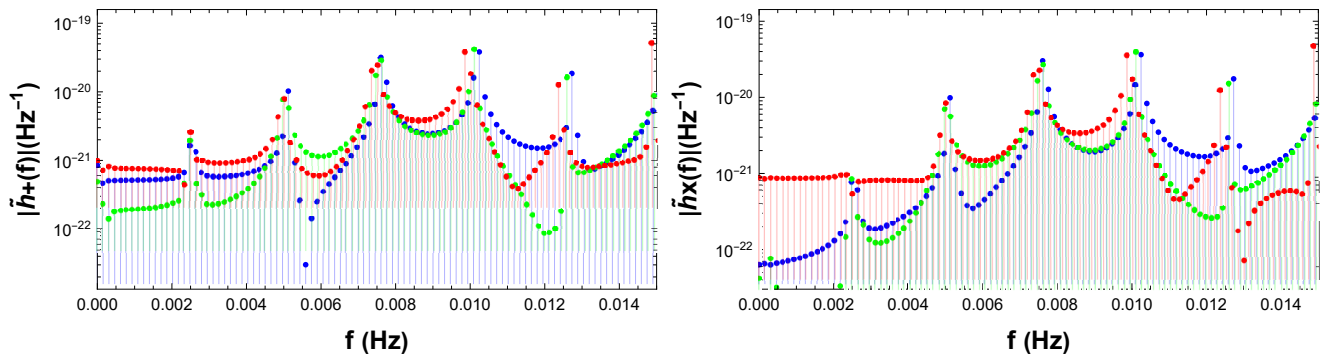


FIG. 7. Fourier spectra  $|\tilde{h}_{+, \times}(f)|$  for the gravitational waveforms in Fig. 5 with zoom-whirl value  $(1, 2, 0)$ . Increasing the quantum-correction parameter shifts the spectral peaks and enhances the high-frequency components, indicating stronger gravitational radiation and modified orbital dynamics.

The frequency spectra are obtained by employing a discrete Fourier transform (DFT) to the time-domain GW-forms, transforming the signal into the frequency domain. This conversion enables a detailed investigation of the signal's frequency content, encoding how the particle's periodic orbital motion modulates the structure of the emitted GWs (see Figs. 6 and 7). The dominant frequencies of these signals lie primarily in the millihertz range, making them especially relevant for space-based detectors such as LISA, Taiji, and Tianqin [14, 15, 116, 118], which are designed to detect low-frequency GWs from EMRIs. The characteristic spectra for different periodic orbits, labeled by the triplet  $(z, w, v)$ , are displayed in Fig. 6, while for various values of  $q_c$  are shown in Fig. 7.

To amplify the visual clarity of the plots for the characteristic strain given in Eq. (4.15), we employed a smoothing procedure to the numerically generated  $h_c(f)$  by performing a running average over 30 frequency bins. Choosing a larger averaging window would further repress numerical noise but could also obscure fine spectral features. As shown in Fig. 8, portions of the characteristic strain corresponding to different orbital configurations  $(z, w, v)$  and values of the quantum-correction parameter  $q_c$  lie above the sensitivity curves of LISA, Taiji, and Tianqin detectors. This means that the corresponding GWs, exhibiting distinctive zoom-whirl features arising from the spacetime above, fall within the detectable range of these future space-based detectors [15, 121, 122]. Such detections would provide a significant opportunity to probe the geometry of spacetime around SMBHs and to test possible quantum-gravity effects through precise GW observations.

## V. DISCUSSIONS AND CONCLUSIONS

The GWs from compact objects orbiting black holes provide a powerful probe of strong-field gravity and the structure of spacetime. In particular, EMRIs are expected to be among the most informative sources for space-based detectors such as LISA, Taiji, and Tian-

qin, as they reveal sensitive information about the background geometry through the small body's orbital motion. Motivated by the above, we have investigated how quantum corrections affect the dynamics of particles around black holes and the resulting gravitational waveforms. Understanding these effects is crucial for determining whether future gravitational-wave observations can detect signatures of quantum gravity or deviations from general relativity in the strong-field regime.

In particular, we investigate periodic orbits and their corresponding waveforms within the limits of quantum-corrected geometry. We analytically solved the geodesics in the background spacetime. After that, we use an exceptional representation [5] to distinguish different types of periodic orbits in quantum-corrected geometry. In this approach, each periodic orbit is described by the parameters  $(z, w, v)$ .

The gravitational waveforms from periodic orbits in quantum-corrected geometry are studied. These results may provide a way to distinguish between black holes in quantum-corrected geometry and the Schwarzschild black hole. We analyze an EMRI system consisting of a test object with mass  $m = 10M_\odot$  following periodic orbits around an SMBH, having mass  $M = 10^6 M_\odot$ . Using the numerical kludge scheme, we investigated the resulting gravitational waveforms by positioning the system at a luminosity distance of  $D_L = 200$  Mpc from the detector, with an inclination angle of  $\iota = \pi/4$  and a longitude of pericenter  $\zeta = \pi/4$ . We demonstrate a clear correlation between the gravitational waveforms emitted by an object orbiting an SMBH and the object's zoom-whirl orbital behaviour. Higher zoom-whirl numbers correspond to more complex waveform substructures. Furthermore, the presence of  $q_c$  has a significant impact on these waveforms. To evaluate the detectability of GWs from EMRIs with periodic orbits, we analyzed their time-domain waveforms using discrete Fourier transforms to extract the frequency spectra. The results indicate that the frequencies of these GWs generally fall within the sensitivity range of space-based detectors. From the spectra, we determined the characteristic strains and observed that,

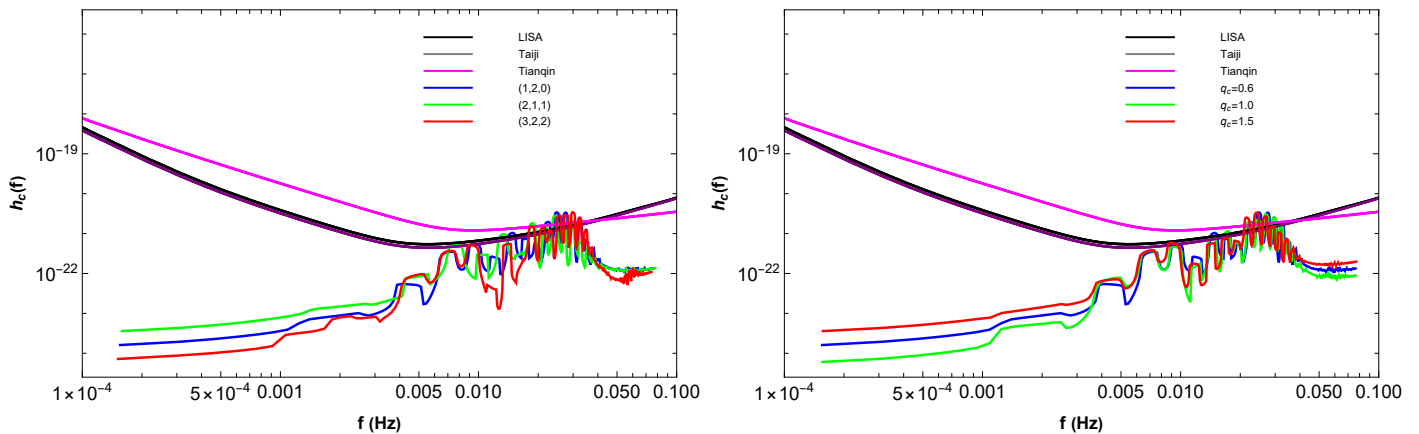


FIG. 8. Characteristics strain of gravitational waveforms of periodic orbits in Figs. 4 (left) and 5 (right). The black, gray, and magenta curves correspond to the sensitivities of the LISA, Taiji, and Tianqin detectors. Portions of the spectra lie above the sensitivity bands, suggesting that these quantum-correction effects could be detectable in future space-based GW observations.

for certain combinations of  $(z, w, v)$ , the strains exceed the sensitivity threshold of LISA, Taiji, and Tianqin. This suggests that space-based gravitational-wave observatories could detect signals from EMRIs with periodic orbits, thereby offering a promising route for exploring SMBHs in spacetimes with quantum corrections. Thus, our study highlights that quantum effects play a critical role in shaping GW signals, offering promising avenues for future observations to probe their influence in strong gravitational fields.

Although we use a particular LQG-inspired metric in our robust approach, the process of identifying periodic orbits using the  $(z, w, v)$  integers and calculating their gravitational-wave signatures may be applied to any static, spherically symmetric black hole spacetime. The Schwarzschild geometry may be corrected differently by various quantum-gravity models; comparing the resulting waveform templates between models may help determine which, if any, are preferred by subsequent observations. A sufficiently high signal-to-noise ratio and a trustworthy template bank that takes into account the orbit's evolution over multiple cycles are necessary for a confident detection, even if our characteristic strain curves are above the noise floors of planned detectors. The adiabatic approximation used here is adequate for short-term waveform modelling, but a complete inspiral-merger-ringdown template—including radiation reaction and higher multipoles—will be essential for parameter estimation. The quantum-corrected black holes considered here may also leave imprints in electromagnetic observations, such as the size of the shadow measured by the Event Horizon Telescope or the frequencies of quasi-normal modes.

In future work, we plan to extend this analysis in several ways. One important step will be to include radiation reaction effects to study how gravitational-wave

emission changes the orbits over time. It will also be beneficial to extend the quadrupole approximation and incorporate higher multipole moments to achieve more accurate waveforms. Another natural extension is to consider rotating quantum-corrected black holes, in which spin may further affect the orbital motion and the emitted radiation. Finally, with future space-based detectors such as LISA [15], Taiji [9, 123], and Tianqin [10, 11], improved waveform templates from such studies could help test deviations from general relativity and explore possible signatures of quantum gravity in the strong-field regime. Future work should assess the precision with which  $q_c$  and the orbital integers can be measured, as well as how degeneracies with other source parameters (e.g., black-hole spin, inclination, and distance) can be broken. A viable approach to cross-validate quantum-gravity phenomena and restrict the underlying theory is to combine gravitational-wave observations with electromagnetic and other gravitational probes, such as pulsar timing. Finally, once these waveforms become available, we will be able to study how future gravitational-wave detectors might test quantum effects on periodic orbits. We aim to address these challenges in upcoming studies.

## ACKNOWLEDGEMENTS

This work is supported by the National Natural Science Foundation of China under Grants No. 12275238, No. 12542053, and No. 11675143, the National Key Research and Development Program under Grant No. 2020YFC2201503, and the Zhejiang Provincial Natural Science Foundation of China under Grants No. LR21A050001 and No. LY20A050002, and the Fundamental Research Funds for the Provincial Universities of Zhejiang in China under Grant No. RF-A2019015.

- 
- [1] B. P. Abbott *et al.* (LIGO Scientific, Virgo), *Phys. Rev. Lett.* **116**, 061102 (2016), [arXiv:1602.03837 \[gr-qc\]](#).
- [2] B. P. Abbott *et al.* (LIGO Scientific, Virgo), *Phys. Rev. D* **93**, 122003 (2016), [arXiv:1602.03839 \[gr-qc\]](#).
- [3] B. P. Abbott *et al.* (LIGO Scientific, Virgo), *Phys. Rev. Lett.* **116**, 241102 (2016), [arXiv:1602.03840 \[gr-qc\]](#).
- [4] B. P. Abbott *et al.* (LIGO Scientific, Virgo), *Phys. Rev. Lett.* **116**, 131103 (2016), [arXiv:1602.03838 \[gr-qc\]](#).
- [5] J. Levin and G. Perez-Giz, *Phys. Rev. D* **77**, 103005 (2008), [arXiv:0802.0459 \[gr-qc\]](#).
- [6] J. Levin, *Class. Quant. Grav.* **26**, 235010 (2009), [arXiv:0907.5195 \[gr-qc\]](#).
- [7] V. Misra and J. Levin, *Phys. Rev. D* **82**, 083001 (2010), [arXiv:1007.2699 \[gr-qc\]](#).
- [8] G. Z. Babar, A. Z. Babar, and Y.-K. Lim, *Phys. Rev. D* **96**, 084052 (2017), [arXiv:1710.09581 \[gr-qc\]](#).
- [9] W.-R. Hu and Y.-L. Wu, *Natl. Sci. Rev.* **4**, 685 (2017).
- [10] J. Luo *et al.* (TianQin), *Class. Quant. Grav.* **33**, 035010 (2016), [arXiv:1512.02076 \[astro-ph.IM\]](#).
- [11] Y. Gong, J. Luo, and B. Wang, *Nature Astron.* **5**, 881 (2021), [arXiv:2109.07442 \[astro-ph.IM\]](#).
- [12] K. Danzmann, *Class. Quant. Grav.* **14**, 1399 (1997).
- [13] B. F. Schutz, *Class. Quant. Grav.* **16**, A131 (1999), [arXiv:gr-qc/9911034](#).
- [14] J. R. Gair, L. Barack, T. Creighton, C. Cutler, S. L. Larson, E. S. Phinney, and M. Vallisneri, *Class. Quant. Grav.* **21**, S1595 (2004), [arXiv:gr-qc/0405137](#).
- [15] P. Amaro-Seoane *et al.* (LISA), (2017), [arXiv:1702.00786 \[astro-ph.IM\]](#).
- [16] A. Maselli, N. Franchini, L. Gualtieri, T. P. Sotiriou, S. Barsanti, and P. Pani, *Nature Astron.* **6**, 464 (2022), [arXiv:2106.11325 \[gr-qc\]](#).
- [17] L. Bian *et al.*, *Sci. China Phys. Mech. Astron.* **69**, 210401 (2024), [arXiv:2505.19747 \[gr-qc\]](#).
- [18] W.-T. Ni, *Sci. Sin. Phys. Mech. Astro.* **54**, 270402 (2024), [arXiv:2409.00927 \[gr-qc\]](#).
- [19] J. Levin and B. Grossman, *Phys. Rev. D* **79**, 043016 (2009), [arXiv:0809.3838 \[gr-qc\]](#).
- [20] P. Bambhaniya, D. N. Solanki, D. Dey, A. B. Joshi, P. S. Joshi, and V. Patel, *Eur. Phys. J. C* **81**, 205 (2021), [arXiv:2007.12086 \[gr-qc\]](#).
- [21] P. Rana and A. Mangalam, *Class. Quant. Grav.* **36**, 045009 (2019), [arXiv:1901.02730 \[gr-qc\]](#).
- [22] C. Liu, C. Ding, and J. Jing, *Commun. Theor. Phys.* **71**, 1461 (2019), [arXiv:1804.05883 \[gr-qc\]](#).
- [23] H.-Y. Lin and X.-M. Deng, *Eur. Phys. J. C* **83**, 311 (2023).
- [24] J.-T. Yao and X. Li, *Phys. Rev. D* **108**, 084067 (2023).
- [25] H.-Y. Lin and X.-M. Deng, *Universe* **8**, 278 (2022).
- [26] Z. C. S. Chan and Y.-K. Lim, *Gen. Rel. Grav.* **57**, 35 (2025), [arXiv:2502.03082 \[gr-qc\]](#).
- [27] R. Wang, F. Gao, and H. Chen, *Annals Phys.* **447**, 169167 (2022).
- [28] H.-Y. Lin and X.-M. Deng, *Annals Phys.* **455**, 169360 (2023).
- [29] S. Haroon and T. Zhu, *Phys. Rev. D* **112**, 044046 (2025), [arXiv:2502.09171 \[gr-qc\]](#).
- [30] A. S. Habibina and H. S. Ramadhan, *Annals Phys.* **448**, 169169 (2023), [arXiv:2205.14635 \[gr-qc\]](#).
- [31] J. Zhang and Y. Xie, *Astrophys. Space Sci.* **367**, 17 (2022).
- [32] H.-Y. Lin and X.-M. Deng, *Eur. Phys. J. Plus* **137**, 176 (2022).
- [33] B. Gao and X.-M. Deng, *Mod. Phys. Lett. A* **36**, 2150237 (2021).
- [34] H.-Y. Lin and X.-M. Deng, *Phys. Dark Univ.* **31**, 100745 (2021).
- [35] X.-M. Deng, *Phys. Dark Univ.* **30**, 100629 (2020).
- [36] Z.-Y. Tu, T. Zhu, and A. Wang, *Phys. Rev. D* **108**, 024035 (2023), [arXiv:2304.14160 \[gr-qc\]](#).
- [37] T.-Y. Zhou and Y. Xie, *Eur. Phys. J. C* **80**, 1070 (2020).
- [38] B. Gao and X.-M. Deng, *Annals Phys.* **418**, 168194 (2020).
- [39] X.-M. Deng, *Eur. Phys. J. C* **80**, 489 (2020).
- [40] M. Azreg-Aïnou, Z. Chen, B. Deng, M. Jamil, T. Zhu, Q. Wu, and Y.-K. Lim, *Phys. Rev. D* **102**, 044028 (2020), [arXiv:2004.02602 \[gr-qc\]](#).
- [41] S.-W. Wei, J. Yang, and Y.-X. Liu, *Phys. Rev. D* **99**, 104016 (2019), [arXiv:1904.03129 \[gr-qc\]](#).
- [42] D. Pugliese, H. Quevedo, and R. Ruffini, *Eur. Phys. J. C* **77**, 206 (2017), [arXiv:1304.2940 \[gr-qc\]](#).
- [43] J. Zhang and Y. Xie, *Eur. Phys. J. C* **82**, 854 (2022).
- [44] J. Healy, J. Levin, and D. Shoemaker, *Phys. Rev. Lett.* **103**, 131101 (2009), [arXiv:0907.0671 \[gr-qc\]](#).
- [45] C.-H. Wang, Y.-P. Zhang, T. Zhu, and S.-W. Wei, (2025), [arXiv:2508.20558 \[gr-qc\]](#).
- [46] M. Alloqulov, S. Shaymatov, B. Ahmedov, and T. Zhu, (2025), [arXiv:2508.05245 \[gr-qc\]](#).
- [47] Z.-L. Wei, J. Zhang, Y. Xie, and P.-L. Yin, *Eur. Phys. J. C* **85**, 698 (2025).
- [48] J. Sharipov, T. Xamidov, Q. Wu, S. Shaymatov, and T. Zhu, (2025), [arXiv:2511.10043 \[gr-qc\]](#).
- [49] S. Yang, Y.-P. Zhang, T. Zhu, L. Zhao, and Y.-X. Liu, *JCAP* **01**, 091 (2025), [arXiv:2407.00283 \[gr-qc\]](#).
- [50] O. Shabbir, M. Jamil, and M. Azreg-Aïnou, *Phys. Dark Univ.* **47**, 101816 (2025), [arXiv:2501.04367 \[gr-qc\]](#).
- [51] E. L. B. Junior, J. T. S. S. Junior, F. S. N. Lobo, M. E. Rodrigues, D. Rubiera-Garcia, L. F. D. da Silva, and H. A. Vieira, *Eur. Phys. J. C* **85**, 557 (2025), [arXiv:2412.00769 \[gr-qc\]](#).

- [52] L. Zhao, M. Tang, and Z. Xu, *Eur. Phys. J. C* **85**, 36 (2025), [arXiv:2411.01979 \[gr-qc\]](#).
- [53] H. Jiang, M. Alloqulov, Q. Wu, S. Shaymatov, and T. Zhu, *Phys. Dark Univ.* **46**, 101627 (2024).
- [54] S. Yang, Y.-P. Zhang, T. Zhu, L. Zhao, and Y.-X. Liu, *Chin. Phys.* **49**, 115107 (2025), [arXiv:2412.04302 \[gr-qc\]](#).
- [55] L. Meng, Z. Xu, and M. Tang, *Eur. Phys. J. C* **85**, 306 (2025), [arXiv:2411.01858 \[gr-qc\]](#).
- [56] Y.-Z. Li, X.-M. Kuang, and Y. Sang, *Eur. Phys. J. C* **84**, 529 (2024), [arXiv:2401.16071 \[gr-qc\]](#).
- [57] Q. Qi, X.-M. Kuang, Y.-Z. Li, and Y. Sang, *Eur. Phys. J. C* **84**, 645 (2024), [arXiv:2407.01958 \[gr-qc\]](#).
- [58] M. Alloqulov, T. Xamidov, S. Shaymatov, and B. Ahmedov, *Eur. Phys. J. C* **85**, 798 (2025), [arXiv:2504.05236 \[gr-qc\]](#).
- [59] C.-H. Wang, X.-C. Meng, Y.-P. Zhang, T. Zhu, and S.-W. Wei, (2025), [10.1088/1475-7516/2025/07/021](#), [arXiv:2502.08994 \[gr-qc\]](#).
- [60] S. Lu and T. Zhu, *Phys. Dark Univ.* **50**, 102141 (2025), [arXiv:2505.00294 \[gr-qc\]](#).
- [61] S. Zare, T. Zhu, L. M. Nieto, S. Lu, and H. Hassanabadi, (2025), [arXiv:2510.05166 \[gr-qc\]](#).
- [62] H. Gong, S. Long, X.-J. Wang, Z. Xia, J.-P. Wu, and Q. Pan, (2025), [arXiv:2509.23318 \[gr-qc\]](#).
- [63] Y.-Z. Li and X.-M. Kuang, (2025), [arXiv:2509.07333 \[gr-qc\]](#).
- [64] S. Choudhury, M. K. Hossain, G. Bauyrzhan, and K. Yezhanov, (2025), [arXiv:2507.00904 \[gr-qc\]](#).
- [65] J. Chen and J. Yang, *Eur. Phys. J. C* **85**, 726 (2025), [arXiv:2505.02660 \[gr-qc\]](#).
- [66] W. Deng, S. Long, Q. Tan, and J. Jing, (2025), [arXiv:2510.24468 \[gr-qc\]](#).
- [67] G.-H. Li, C.-K. Qiao, and J. Tao, (2025), [arXiv:2510.24989 \[gr-qc\]](#).
- [68] T. Zahra, O. Shabbir, B. Majeed, M. Jamil, J. Rayimbaev, and A. Shermatov, (2025), [arXiv:2510.22761 \[gr-qc\]](#).
- [69] F. Ahmed, Q. Wu, S. G. Ghosh, and T. Zhu, (2025), [arXiv:2511.08456 \[gr-qc\]](#).
- [70] C. Zhang and T. Zhu, (2025), [arXiv:2511.14080 \[gr-qc\]](#).
- [71] M. Alloqulov, S. Shaymatov, B. Ahmedov, and T. Zhu, (2025), [arXiv:2511.15237 \[gr-qc\]](#).
- [72] S. Lu, H.-J. Lin, T. Zhu, Y.-X. Liu, and X. Zhang, (2025), [arXiv:2512.11911 \[gr-qc\]](#).
- [73] A. Ashtekar and E. Bianchi, *Rept. Prog. Phys.* **84**, 042001 (2021), [arXiv:2104.04394 \[gr-qc\]](#).
- [74] R. Penrose, *Phys. Rev. Lett.* **14**, 57 (1965).
- [75] A. Ashtekar and J. Lewandowski, *Class. Quant. Grav.* **21**, R53 (2004), [arXiv:gr-qc/0404018](#).
- [76] R. A. Konoplya and O. S. Stashko, *Phys. Rev. D* **111**, 104055 (2025), [arXiv:2408.02578 \[gr-qc\]](#).
- [77] Y.-H. Shu and J.-H. Huang, *Phys. Lett. B* **864**, 139411 (2025), [arXiv:2412.05670 \[gr-qc\]](#).
- [78] M. Skvortsova, *Eur. Phys. J. C* **85**, 854 (2025), [arXiv:2411.06007 \[gr-qc\]](#).
- [79] W. Liu, D. Wu, and J. Wang, *Phys. Lett. B* **858**, 139052 (2024), [arXiv:2408.05569 \[gr-qc\]](#).
- [80] H. Liu, M.-Y. Lai, X.-Y. Pan, H. Huang, and D.-C. Zou, *Phys. Rev. D* **110**, 104039 (2024), [arXiv:2408.11603 \[gr-qc\]](#).
- [81] Y. Du, Y. Liu, and X. Zhang, *JCAP* **05**, 045 (2025), [arXiv:2411.13316 \[gr-qc\]](#).
- [82] Z. Ban, J. Chen, and J. Yang, *Eur. Phys. J. C* **85**, 878 (2025), [arXiv:2411.09374 \[gr-qc\]](#).
- [83] Y. Wang, A. Vachher, Q. Wu, T. Zhu, and S. G. Ghosh, *Eur. Phys. J. C* **85**, 302 (2025), [arXiv:2410.12382 \[astro-ph.CO\]](#).
- [84] U. Uktamov, M. Alloqulov, S. Shaymatov, T. Zhu, and B. Ahmedov, *Phys. Dark Univ.* **47**, 101743 (2025), [arXiv:2412.01809 \[gr-qc\]](#).
- [85] K. Akiyama *et al.* (Event Horizon Telescope), *Astrophys. J. Lett.* **875**, L1 (2019), [arXiv:1906.11238 \[astro-ph.GA\]](#).
- [86] K. Akiyama *et al.* (Event Horizon Telescope), *Astrophys. J. Lett.* **930**, L12 (2022), [arXiv:2311.08680 \[astro-ph.HE\]](#).
- [87] C. Rovelli, *PoS QGGS2011*, 003 (2011), [arXiv:1102.3660 \[gr-qc\]](#).
- [88] A. Perez, *Rept. Prog. Phys.* **80**, 126901 (2017), [arXiv:1703.09149 \[gr-qc\]](#).
- [89] A. Alonso-Bardaji, D. Brizuela, and R. Vera, *Phys. Lett. B* **829**, 137075 (2022), [arXiv:2112.12110 \[gr-qc\]](#).
- [90] A. Alonso-Bardaji, D. Brizuela, and R. Vera, *Phys. Rev. D* **106**, 024035 (2022), [arXiv:2205.02098 \[gr-qc\]](#).
- [91] G. Fu, D. Zhang, P. Liu, X.-M. Kuang, and J.-P. Wu, *Phys. Rev. D* **109**, 026010 (2024), [arXiv:2301.08421 \[gr-qc\]](#).
- [92] Z. S. Moreira, H. C. D. Lima Junior, L. C. B. Crispino, and C. A. R. Herdeiro, *Phys. Rev. D* **107**, 104016 (2023), [arXiv:2302.14722 \[gr-qc\]](#).
- [93] S. V. Bolokhov, *Phys. Rev. D* **110**, 024010 (2024), [arXiv:2311.05503 \[gr-qc\]](#).
- [94] D. M. Gingrich, *Phys. Rev. D* **110**, 084045 (2024), [arXiv:2404.04447 \[gr-qc\]](#).
- [95] S. Yang, W.-D. Guo, Q. Tan, L. Zhao, and Y.-X. Liu, *Phys. Rev. D* **110**, 064051 (2024), [arXiv:2406.15711 \[gr-qc\]](#).
- [96] L. Zhao, M. Tang, and Z. Xu, *Eur. Phys. J. C* **84**, 971 (2024), [arXiv:2403.18606 \[gr-qc\]](#).
- [97] Y. Dong, *Nucl. Phys. B* **1005**, 116612 (2024).
- [98] A. R. Soares, R. L. L. Vitória, and C. F. S. Pereira, *Phys. Rev. D* **110**, 084004 (2024), [arXiv:2408.03217 \[gr-qc\]](#).
- [99] F. Ahmed, *Int. J. Geom. Meth. Mod. Phys.* **22**, 2450336 (2025), [arXiv:2409.05897 \[gr-qc\]](#).
- [100] H.-Y. Shi and T. Zhu, *Eur. Phys. J. C* **84**, 814 (2024).
- [101] F. C. Sobrinho, H. A. Borges, I. P. R. Baranov, and S. Carneiro, *Class. Quant. Grav.* **40**, 145003 (2023), [arXiv:2212.11199 \[gr-qc\]](#).
- [102] C. Liu, T. Zhu, Q. Wu, K. Jusufi, M. Jamil, M. Azreg-Aïnou, and A. Wang, *Phys. Rev. D* **101**, 084001 (2020), [Erratum: *Phys. Rev. D* **103**, 089902 (2021)],

- arXiv:2003.00477 [gr-qc].
- [103] T. Zhu and A. Wang, *Phys. Rev. D* **102**, 124042 (2020), arXiv:2008.08704 [gr-qc].
  - [104] J.-M. Yan, Q. Wu, C. Liu, T. Zhu, and A. Wang, *JCAP* **09**, 008 (2022), arXiv:2203.03203 [gr-qc].
  - [105] J.-M. Yan, C. Liu, T. Zhu, Q. Wu, and A. Wang, *Phys. Rev. D* **107**, 084043 (2023), arXiv:2302.10482 [gr-qc].
  - [106] C. Liu, H. Siew, T. Zhu, Q. Wu, Y. Sun, Y. Zhao, and H. Xu, *JCAP* **11**, 096 (2023), arXiv:2305.12323 [gr-qc].
  - [107] H.-X. Jiang, C. Liu, I. K. Dihingia, Y. Mizuno, H. Xu, T. Zhu, and Q. Wu, *JCAP* **01**, 059 (2024), arXiv:2312.04288 [gr-qc].
  - [108] H.-X. Jiang, I. K. Dihingia, C. Liu, Y. Mizuno, and T. Zhu, *JCAP* **05**, 101 (2024), arXiv:2402.08402 [astro-ph.HE].
  - [109] T. Xamidov, P. Sheoran, S. Shaymatov, and T. Zhu, *JCAP* **03**, 053 (2025), arXiv:2412.03885 [gr-qc].
  - [110] T. Xamidov, S. Shaymatov, B. Ahmedov, and T. Zhu, (2025), arXiv:2503.06750 [gr-qc].
  - [111] G. Fatima, T. Zhu, F. Javed, A. Waseem, and G. Mustafa, *Eur. Phys. J. C* **85**, 208 (2025).
  - [112] A. R. Soares, C. F. S. Pereira, R. L. L. Vitória, and E. M. Rocha, *Phys. Rev. D* **108**, 124024 (2023), arXiv:2309.05106 [gr-qc].
  - [113] J. Levin and G. Perez-Giz, *Phys. Rev. D* **79**, 124013 (2009), arXiv:0811.3814 [gr-qc].
  - [114] S. Chandrasekhar, *The mathematical theory of black holes* (1985).
  - [115] S. A. Hughes, *Phys. Rev. D* **61**, 084004 (2000), [Erratum: *Phys.Rev.D* 63, 049902 (2001), Erratum: *Phys.Rev.D* 65, 069902 (2002), Erratum: *Phys.Rev.D* 67, 089901 (2003), Erratum: *Phys.Rev.D* 78, 109902 (2008), Erratum: *Phys.Rev.D* 90, 109904 (2014)], arXiv:gr-qc/9910091.
  - [116] L. Barack and C. Cutler, *Phys. Rev. D* **69**, 082005 (2004), arXiv:gr-qc/0310125.
  - [117] S. Isoyama, R. Fujita, A. J. K. Chua, H. Nakano, A. Pound, and N. Sago, *Phys. Rev. Lett.* **128**, 231101 (2022), arXiv:2111.05288 [gr-qc].
  - [118] S. Babak, H. Fang, J. R. Gair, K. Glampedakis, and S. A. Hughes, *Phys. Rev. D* **75**, 024005 (2007), [Erratum: *Phys.Rev.D* 77, 04990 (2008)], arXiv:gr-qc/0607007.
  - [119] S. A. Hughes, *Class. Quant. Grav.* **18**, 4067 (2001), arXiv:gr-qc/0008058.
  - [120] K. S. Thorne, *Rev. Mod. Phys.* **52**, 299 (1980).
  - [121] J. R. Gair, S. Babak, A. Sesana, P. Amaro-Seoane, E. Barausse, C. P. L. Berry, E. Berti, and C. Sopuerta, *J. Phys. Conf. Ser.* **840**, 012021 (2017), arXiv:1704.00009 [astro-ph.GA].
  - [122] S. Babak, J. Gair, A. Sesana, E. Barausse, C. F. Sopuerta, C. P. L. Berry, E. Berti, P. Amaro-Seoane, A. Petiteau, and A. Klein, *Phys. Rev. D* **95**, 103012 (2017), arXiv:1703.09722 [gr-qc].
  - [123] W.-H. Ruan, Z.-K. Guo, R.-G. Cai, and Y.-Z. Zhang, *Int. J. Mod. Phys. A* **35**, 2050075 (2020), arXiv:1807.09495 [gr-qc].